Surv Geophys (2012) 33:483–501
DOI 10.1007/s10712-012-9192-0

Influence of the Precipitating Energetic Particles on Atmospheric Chemistry and Climate

E. Rozanov · M. Calisto · T. Egorova · T. Peter · W. Schmutz

Received: 2 September 2011 / Accepted: 14 April 2012 / Published online: 3 May 2012

Abstract We evaluate the influence of the galactic cosmic rays (GCR), solar proton events (SPE), and energetic electron precipitation (EEP) on chemical composition of the atmosphere, dynamics, and climate using the chemistry-climate model SOCOL. We have carried out two 46-year long runs. The reference run is driven by a widely employed forcing set and, for the experiment run, we have included additional sources of NO_x and HO_x caused by all considered energetic particles. The results show that the effects of the GCR, SPE, and EEP fluxes on the chemical composition are most pronounced in the polar mesosphere and upper stratosphere; however, they are also detectable and statistically significant in the lower atmosphere consisting of an ozone increase up to 3 % in the troposphere and ozone depletion up to 8 % in the middle stratosphere. The thermal effect of the ozone depletion in the stratosphere propagates down, leading to a warming by up to 1 K averaged over 46 years over Europe during the winter season. Our results suggest that the energetic particles are able to affect atmospheric chemical composition, dynamics, and climate.

Keywords Energetic particles · Atmospheric chemistry · Dynamics · Climate · Modeling

1 Introduction

Understanding of the past climate change and forecasting of the future climate requires a clear quantification of the contribution from all relevant anthropogenic and natural forcing. The contribution of energetic particles to climate change is a not well known and

E. Rozanov (✉) · T. Egorova · W. Schmutz
Physikalisch-Meteorologisches Observatorium Davos/World Radiation Center, Davos, Switzerland
e-mail: e.rozanov@pmodwrc.ch

E. Rozanov · T. Peter
Institute for Atmospheric and Climate Science ETH, Zurich, Switzerland

M. Calisto
International Space Science Institute (ISSI), Bern, Switzerland

controversial issue among many other natural factors. Therefore, the energetic particles were not taken into account neither for the extensive evaluation of the ozone trends (Eyring et al. 2007; SPARC CCMVal 2010) nor for the analysis of the climate changes (IPCC 2007). The aim of this paper is to analyze the impact of the energetic particles and convince the community that the energetic particles are able to change the mean state of the atmospheric chemistry and climate.

According to their sources and energy spectra, precipitating energetic particles can be divided into galactic cosmic rays (GCR), solar protons (SP), and low- and high-energy electrons (LEE and HEE). All these particles are able to ionize neutral molecules (e.g., N_2 and O_2) in the Earth's atmosphere, but the distribution of ionization rates in space and time depend on the particle type because of their interactions with the variable heliomagnetic and geomagnetic fields.

The GCR originate from outside of the solar system and consist mostly of protons with kinetic energy spanning the interval from 1 MeV up to at least 5×10^{13} MeV (e.g., Bazilevskaya et al. 2008). The GCR are able to ionize neutral molecules in the Earth's upper-to-middle atmosphere almost everywhere, but the penetration depth increases toward the polar atmosphere, where the effect of the geomagnetic field on charged particle motion means that more, and lower-energy, particles reach the atmosphere. The ionization rate by GCR reaches its maximum around 15 km (Usoskin et al. 2010). The ionization in the lower troposphere near the equator can only be produced by highly (>15 GeV) energetic particles. Modulation of the cosmic ray flux by the solar activity is more pronounced for less energetic (<1 GeV) particles, while a highly (above 100 GeV) energetic GCR flux remains almost intact (e.g., Bazilevskaya et al. 2008). This modulation leads to a pronounced variability of the GCR-induced ionization rate, which maximizes during the minimum of the solar activity cycles mostly over high geomagnetic latitudes (Usoskin and Kovaltsov 2006; Calisto et al. 2011).

Solar energetic protons are generated in the solar corona or in interplanetary space by coronal mass ejections (CME) driven shocks and/or during impulsive energy releases in solar flares reaching kinetic energy typically up to 500 MeV (Reames 1999; Cane et al. 2006).

After their generation and propagation, the protons drift along the magnetic lines ionizing the thermosphere (>80 km), mesosphere (50–80 km), and, in some extreme cases, the stratosphere (15–50 km) mostly over the polar regions (Jackman et al. 2008 and references therein). Solar proton events (SPE) are sporadic, but their frequency tends to increase during the maximum activity of the Sun when the probability of CME is higher, while their fluence has an opposite tendency (Barnard and Lockwood 2011).

Low-energy (1–30 keV) auroral electrons almost continuously precipitate from the Earth's magnetospheric plasmasheet (Brasseur and Solomon 2005). Their energy is mostly deposited in the lower thermosphere (above 90 km) inside the auroral ovals located over the 60°–75° geomagnetic latitude band (Baker et al. 2001; Barth et al. 2003). The strength of the auroral electron precipitation defined as the total hemispheric precipitating energy flux depends on the geomagnetic activity level and reaches its maximum during the declining phase of the solar activity cycle (Emery et al. 2008; Marsh et al. 2007).

High-energy (from 30 keV up to several MeV) electrons originate from the outer radiation belts (e.g., Bazilevskaya et al. 2008). Their precipitation to the atmosphere is caused by complex wave-particle interaction and mostly confined to the subauroral latitudes (Millan and Thorne 2007; Lam et al. 2010). The penetration depth of high-energy electrons varies from 90 km for 30 keV electrons and down to 50 km for 2 MeV electrons (Turunen et al. 2009). Meredith et al. (2011) pointed out that their fluxes can be substantially enhanced during the geomagnetic perturbations associated with enhanced

dynamical pressure of the solar wind caused by CMEs and high-speed solar wind streams (HSSWS). The relation of high-energy precipitation events to solar activity is not well defined yet, but in general, the frequency of the CME-driven electron precipitation should be higher around solar maximum, while the probability of HSSWS-driven electron precipitation increases considerably when coronal holes extend to low latitudes, such that HSSWS impact on Earth, which occurs most often in the declining phase of the solar cycle (Richardson et al. 2000). The ionization induced by the energetic particle precipitation leads to the production of nitrogen and hydrogen oxides via the chain of chemical processes involving electrons, positive, and negative ions (Rusch et al. 1981; Aikin 1994; Solomon et al. 1981; Turunen et al. 2009; Egorova et al. 2011). The subsequent fate of the nitrogen and hydrogen oxides produced by particles depends on their lifetime. The response of the short-lived HO_x is highly localized in time and space and can be observed only during the particle precipitation event in the region where the ionization occurs. NO_x is more stable and can be transported by atmospheric winds; therefore, NO_x enhancement can be observed after the event has started and far from the production area. This mechanism is particularly important during the polar night when the lifetime of NO_x produced by solar protons and magnetospheric electrons is longer and they are transported by the downward air motion inside the polar vortex toward the middle stratosphere (Funke et al. 2005; Seppälä et al. 2007a). The NO_x and HO_x enhancement caused by the particles has important implications for the ozone concentration in the stratosphere. Below the tropopause, that is, below about 15 km, the ozone production can be enhanced by additional NO_x due to photosmog reactions (e.g., Wang et al. 1998), while in the middle atmosphere, additional amount of active nitrogen and hydrogen oxides intensifies ozone destruction (Brasseur and Solomon 2005). The ozone changes in the stratosphere lead to the perturbation of the net radiative heating and temperature regime, which can have implications for the dynamical state of the vortex and surface climate (Gray et al. 2010).

Many of the theoretically expected particle effects were confirmed by observation data analysis. The enhancement of NO in the auroral zone has been observed by SNOE measurements (Barth et al. 2001). NO_x and HO_x enhancement in the mesosphere and stratosphere due to in situ ionization was detected by satellite measurements mostly during powerful precipitation events (e.g., López-Puertas et al. 2005; Seppälä et al. 2007b; Damiani et al. 2008; Funke et al. 2011; Verronen et al. 2011). The enhancement of NO_x in the stratosphere after substantial geomagnetic perturbation was detected by many groups (e.g., Callis et al. 1998; Siskind et al. 2000; Randall et al. 2007; Clilverd et al. 2009). Its proper attribution, however, is still under investigations, because the separation of the direct production and transport of NO_x from above is not straightforward due to incomplete information of the energy spectrum of precipitating particles (López-Puertas et al. 2006, Sinnhuber et al. 2011). The production of NO_x and HO_x by GCR has not yet been confirmed observationally due to a rather small magnitude of the enhancement in the polar upper troposphere/lower stratosphere (UTLS) region, where the effects of GCR should be the most pronounced. The ozone depletion in the polar mesosphere and stratosphere after intensive SPE was observed by different satellite instruments (López-Puertas et al. 2005; Seppälä et al. 2007b; Funke et al. 2011). Significant correlation of the surface air temperature with the level of geomagnetic activity, which is represented by the Ap index, was discovered in the reanalysis data by Seppälä et al. (2009).

The modeling of particle effects has been mostly aimed at the study of short-term powerful particle precipitation events, which are characterized by a large signal to noise ratio and therefore can be readily identified in the model results and compared to observations. A large number of simulations of the atmospheric changes caused by SPE have

been performed using models of different complexity (see Jackman et al. 2008 and references therein, Reddmann et al. 2010, Egorova et al. 2011) and a successful reproduction of the main observed features have been recently reported by Funke et al. (2011).

During the last years, attempts to estimate the importance of the particle precipitation for the long-term changes of ozone and climate using sophisticated chemistry-climate models (CCM) have been made. Langematz et al. (2005) found significant response of the stratospheric ozone caused by low-energy electrons. Rozanov et al. (2005) simulated the ozone and climate response to enhancement of nitrogen and hydrogen oxides caused by electrons with low and high energies and found significant response of the atmosphere and surface climate. Despite the application of an idealized forcing and absence of other particle types, these studies inspired further investigations in this direction. Jackman et al. (2009) estimated the long-term climate influence of the SPE and did not find pronounced response of the total column ozone and climate, which is expected due to low frequency of powerful SPE and a lack of continuous effects of GCR and energetic electrons as well as a relatively stable solar activity level during the considered period. The importance of NO_x production by auroral electrons was illustrated by Marsh et al. (2007) using a parameterization of the ionization rates based on geomagnetic Kp index, which classifies solar particle effects on the Earth's magnetic field. Baumgaertner et al. (2009, 2011) developed a parameterization for the NO_x production by low-energy electrons and studied the atmospheric response to the level of geomagnetic activity. They found substantial depletion of ozone in the polar winter stratosphere ($\sim$15–50 km) followed by a distinctive surface air temperature and sea-level pressure responses in agreement with previous investigations. Calisto et al. (2011) simulated the effects of the GCR using the CCM SOCOL v2.0 with continuously varying boundary conditions (transient mode) with the latest parameterization (Usoskin et al. 2010) of the GCR-induced ionization rates. They reported small ($\sim$3 %) but statistically significant ozone depletion in the Northern hemisphere lower polar stratosphere and a winter time warming in the eastern part of Europe and in Russia. A first attempt to include several types of precipitating particles (GCR, SPE, and low- to middle-energy electrons) has been made by Semeniuk et al. (2011). They reported a wintertime polar stratosphere ozone reduction up to 10 % and substantial dynamical changes over the Southern hemisphere caused by the energetic particles. Unfortunately, Semeniuk et al. (2011) did not analyze the surface air temperature response and the contribution of all energetic particles to climate change. The results presented in this paper and the fact that just Semeniuk et al. (2011) have investigated the influence of the GCRs, SPEs, and EEPs clearly show that more simulations driven by all known energetic particles are necessary to estimate their significance for the ozone trends and climate change analysis.

In this paper, we study the combined effects of the GCR, solar protons, and low-energetic electrons using the global chemistry-climate model SOCOL v2.0 (Schraner et al. 2008) focusing on the changes of atmospheric chemistry and dynamics caused by the inclusion of additional NO_x and HO_x sources. The description of the model and experimental setup including the applied parameterizations of the NO_x and HO_x production by different energetic particles are presented in Sect. 2. The results of the reference and experimental runs are analyzed in Sect. 3. Section 4 presents the summary and an outlook.

2 Model Description and Experimental Setup

The CCM SOCOL consists of the global circulation model MA-ECHAM4 and the chemistry-transport model MEZON. MA-ECHAM4 (Manzini et al. 1997) is a spectral

model with T30 horizontal truncation, that is, the model has a horizontal resolution resulting in a grid spacing of about 3.75°; in the vertical direction, the model has 39 levels in a hybrid sigma-pressure coordinate system spanning the model atmosphere from the surface to 0.01 hPa.

The chemical-transport model MEZON (Rozanov et al. 1999; Egorova et al. 2003) exploits the same vertical and horizontal resolution and treats 41 chemical species of the oxygen, hydrogen, nitrogen, carbon, chlorine and bromine groups, which are coupled by 140 gas-phase reactions, 46 photolysis reactions and 16 heterogeneous reactions in/on aqueous sulfuric acid aerosols, water ice, and nitric acid trihydrate (NAT). The original version of the CCM SOCOL was described by Egorova et al. (2005). An extensive evaluation of the CCM SOCOL (Egorova et al. 2005; Eyring et al. 2007) revealed model deficiencies in the chemical-transport module and led to the development of the CCM SOCOL v2.0. The new features of the SOCOLv2.0 are the following: (1) all species are transported separately; (2) the mass conservation after each semi-Lagrangian transport step is maintained by the correction coefficients calculated for the chlorine, bromine, and nitrogen families instead for individual family members, but then applied to each individual species; (3) the mass fixer is applied to ozone only over the latitude band 40°S–40°N to avoid artificial mass loss in the polar lower stratosphere; (4) the water vapor removal by the highest ice clouds (between 100 hPa ($\sim$16 km) and the tropical cold point tropopause) is explicitly taken into account to prevent an overestimation of stratospheric water content; (5) the list of ozone-depleting substances is extended to 15 for the chemical treatment, while for the transport they are still clustered into three tracer groups; (6) the heterogeneous chemistry module was updated to include HNO_3 uptake by aqueous sulfuric acid aerosols, a parameterization of the liquid-phase reactive uptake coefficients and the NAT particle number densities are limited by an upper boundary of 5×10^{-4} cm^{-3} to take account of the fact that observed NAT clouds are often strongly supersaturated.

A comprehensive description of the CCM SOCOL v2.0 is presented by Schraner et al. (2008). The evaluation of CCM SOCOL in the framework of SPARC CCMVal-2 intercomparison campaign (SPARC CCMVal, 2010) showed substantial improvement of the representation of the transport and chemical processes in the model; however, some shortcomings in the simulation of gas transport still remains. It also showed that the internal variability of our model was found to be in good agreement with reanalyzed data.

The ionization rates due to the GCR have been parameterized using the recently developed CRAC:CRII (Cosmic Ray induced Cascade: Application for Cosmic Ray Induced Ionization) model extended toward the upper atmosphere (Usoskin et al. 2010). The model is based on a Monte Carlo simulation of the atmospheric cascade and reproduces the observed data within 10 % accuracy in the troposphere and lower stratosphere (Bazilevskaya et al. 2008; Usoskin et al. 2010). In the mesosphere ($\sim$50–80 km), the agreement between observed and simulated ionizations rates are not good because the ionization by other sources (solar radiation, precipitating soft particles of magnetospheric origin, etc.) becomes at least as important as by GCRs. The results of the CRAC:CRII model are parameterized (see Usoskin and Kovaltsov 2006) to give ion pair production rate as a function of the altitude (quantified via the barometric pressure), geomagnetic latitude (quantified via geomagnetic cutoff rigidity), and solar activity (quantified via the modulation potential θ).

For the solar protons, we applied daily averaged ionization rates from 1963 to 2008 compiled by Charles Jackman and available from the SOLARIS website (URL: http://www.geo.fu-berlin.de/en/met/ag/strat/forschung/SOLARIS/Input_data/ index.html) as a function of pressure between 888 hPa ($\sim$1 km above ground level) and 8×10^{-5} hPa

(~115 km). The ionization rates were introduced to the model over the polar region from 60° to 90° geomagnetic latitudes. The area of ionization by high-energy (>10 MeV) protons is well inside the model domain (Turunen et al. 2009) and their effects should be properly accounted for. Despite the fact that the model used in this study cannot directly include the production of NO_x and HO_x above 80 km (i.e. outside the model domain) by low-energy protons and concomitant electrons (Wissing et al. 2010) Funke et al. (2011) mention in their paper that the importance of electron contribution is still under discussion. Therefore, instead of the direct production, we have to parameterize the influx of NO_x produced by energetic electrons above the model top. We apply the Baumgaertner et al. (2009) parameterization of nitrogen oxides influx into the model domain based on the empirical relation with geomagnetic Ap index, which represents the geomagnetic activity using their "average excess NO_x" mode. The values of the Ap index were obtained from the National Geophysical Data Center (ftp://ftp.ngdc.noaa.gov). It has been shown by Funke et al. (2005) that the effect of the energetic electrons on the mesosphere and stratosphere is confined to the polar vortex. Therefore, the minimum absolute latitude of 55° has been used, that is, the products of the ionization by energetic electrons enter our model domain only at high latitudes. Further, downward propagation of ionization products depends on the presence of polar vortices and appropriate vertical transport, which guarantees that the ionization products properly affect the lower mesosphere and stratosphere. The model currently does not include high (>50 keV)-energy electrons that deposit their energy below 80 km because a proper parameterization for the high-energy electrons is not available. The lack of this process in the model can be justified by a small contribution of high-energy electron precipitation events to the total NO_x production by particles estimated by Sinnhuber et al. (2011) from observational data.

The GCR and SPE ionization rates cannot be directly used in the CCM SOCOL, which has no explicit treatment of ion chemistry; therefore, it is necessary to convert the ionization into the NO_x and HO_x production rates. Following Porter et al. (1976), we assumed that 1.25 nitrogen atoms are produced per ion pair, and 45 % of this is assumed to yield ground-state atomic nitrogen, while 55 % is assumed to go into $N(^2D)$ with instantaneous conversion to NO (see Introduction). The production of HO_x has been studied by Solomon et al. (1981) with a 1-D time-dependent model of neutral and ion chemistry. They parameterized the number of odd hydrogen particles produced per ion pair as a function of altitude and ionization for daytime, polar summer conditions of temperature, air density, and solar zenith angle. We implement these parameterizations in the CCM SOCOL to take into account the production of NO_x and HO_x induced by GCR and SPE from the ground up to the height of 0.01 hPa barometric pressure (altitude of ~ 80 km). The errors associated with this approach are within 10–20 % (Egorova et al. 2011), which is comparable with the accuracy of ionization rate calculations.

For this study, we have carried out two 46-year long runs with the CCM SOCOL v2.0 from 1960 to 2005. The reference run has been performed without the influence of the energetic particles, while the experimental run includes additional sources of NO_x and HO_x caused by the influence of GCR, SPE, and EEP. Both model experiments are driven by time-varying boundary conditions for the source gases, aerosol loading, solar irradiance, sea surface temperatures, and sea ice concentration identical to the CCMVal-2 REF-B1 experiment (SPARC CCMVal 2010; Morgenstern et al. 2010). The numerical experiments performed here are similar to the experiments described by Calisto et al. (2011), but the additional NO_x and HO_x sources are extended to take into account SPE and EEP in addition to GCR. The model integration time increases to 46 years, compared to Calisto et al. (2011), which had an integration time of 27 years. Our simulations are also close to the

experiments analyzed by Semeniuk et al. (2011). These papers will be referred to as CA11 and SE11 hereafter.

3 Results

In this section, we analyze the difference between the climatological state of the model run with the influence of the energetic particles (experimental run) and the run without the influence of the energetic particles (reference run). All resulting changes in the atmospheric state are taken into account for the calculation of statistical significance, which is estimated using the Student's t test.

3.1 Nitrogen Oxides

Figure 1 illustrates the annual mean zonal mean NO_x response to the influence of the GCR, SPE, and EEP as a relative deviation of the experimental run from the reference run. The GCR, SPE, and EEP produce substantial amounts of NO_x. The simulated NO_x increase is strongest in the mesosphere. The pronounced NO_x enhancement of more than 1,000 % in the polar mesosphere (approximately 50–80 km) is an expected result of the direct NO_x production by the energetic particles. A significant enhancement of up to 400 % is depicted in the mesosphere over the middle and low latitudes, which can be attributed to the meridional transport. CA11 and SE11 demonstrated that there is no significant NO_x response to GCR in this area. EEP and SPE operate only over the polar regions. This effect is not really foreseen due to rather short NO_x lifetime outside the polar night area, but a similar feature has also been obtained by SE11. This NO_x enhancement can be explained by a rather fast transport in the mesosphere in comparison with the chemical lifetime of NO_x. The reliability of this mechanism is partially confirmed by the shape of the mesospheric NO_x enhancement which is not symmetrical in the latitudinal direction, showing more intensive increase in the Northern hemisphere, which is consistent with more dynamically active boreal cold seasons leading to more intensive meridional transport there. The southern polar hemisphere shows at about 10 hPa (~32 km), and at about

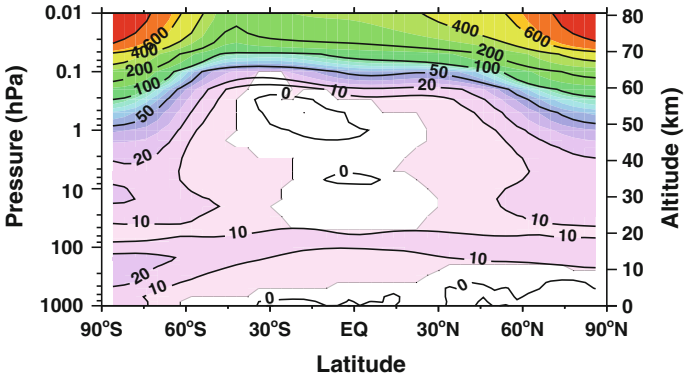

Fig. 1 Annual mean response of zonal mean NO_x, (%) to GCR, SPE, and EEP. Results are averaged from 1960 to 2005. *Solid contours* indicate positive changes. The *contours* are plotted for: 10, 20, 50, 100, 200, 400, 600, and 1,000 %. *Color* pattern indicates the regions where the changes are judged statistically significant at or better than 10 % level

200 hPa (~12 km), another statistical significant increase for NO_x. The enrichment at 10 hPa is a result of the combined SPE and EEP influence, whereas the NO_x at 200 hPa has been formed by GCR, which is also visible in the CA11 results. The enhancement of the tropospheric NO_x in the northern hemisphere is less than 10 % and statistically insignificant. This result does not agree with SE11, which reported a large (>30 %) and statistically significant increase in the tropospheric NO_x in both hemispheres. The reasons for this disagreement are not completely clear, but most probably it is the result of the simplified treatment of the tropospheric chemistry in the model applied by SE11 and the absence of other natural and anthropogenic NO_x sources in the troposphere.

The seasonal behavior of NO_x enhancement due to energetic particles averaged over the Northern and Southern polar region (60°–90°) is illustrated in Figs. 2 and 3, respectively.

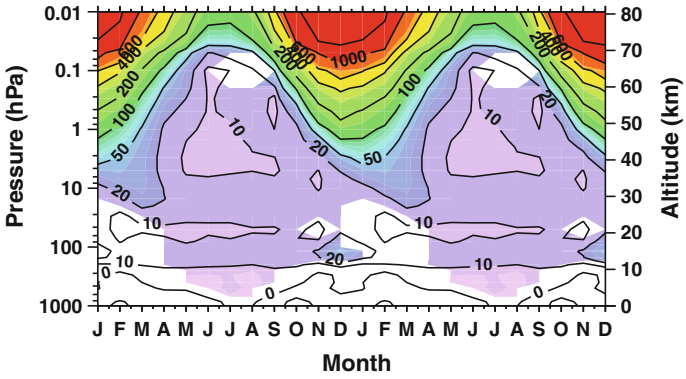

Fig. 2 Monthly mean response of zonal mean NO_x, (%) to GCR, SPE, and EEP averaged over 60°–90°N. Results are averaged from 1960 to 2005. *Solid contours* indicate positive changes. The *contours* are plotted for: 10, 20, 50, 100, 200, 400, 600, 1,000, and 2,000 %. *Color* pattern indicates the regions where the changes are judged statistically significant at or better than 10 % level. Twelve months of the monthly run climatology are repeated

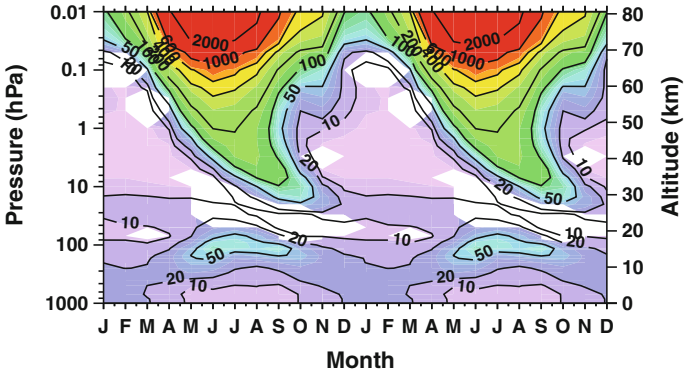

Fig. 3 Monthly mean response of zonal mean NO_x, (%) to GCR, SPE, and EEP averaged over 60°–90°S. Results are averaged from 1960 to 2005. *Solid contours* indicate positive changes. The *contours* are plotted for: 10, 20, 50, 100, 200, 400, 600, 1,000, and 2,000 %. *Color* pattern indicates the regions where the changes are judged statistically significant at or better than 10 % level. Twelve months of the monthly run climatology are repeated

The results in the mesosphere show an expected maximum response during the hemispheric winter when it is cold and dark. During this time, the downward propagation of thermospheric NO_x inside the vortex can operate and this NO_x, therefore, will not be depleted by solar irradiance. Stronger vortex and more intensive downward transport in the Southern hemisphere lead to a deeper penetration of the thermospheric NO_x. In this area, an increase of 50 % is visible down to 20 hPa (~26 km), while in the Northern hemisphere it reaches only 3 hPa (~40 km). The NO_x increase above 10 hPa (~32 km) during the hemispheric summer is smaller (only up to 100 %) due to the absence of the thermospheric NO_x influx and NO_x relaxation to the chemical equilibrium in the presence of the sunlight via NO photolysis followed by the cannibalistic reaction $N + NO \rightarrow N_2 + O$ (Brasseur and Solomon 2005). Similar distribution in the polar middle atmosphere has been obtained by SE11.

The seasonal cycle of NO_x enhancement is also visible in an altitude range from 12 km up to 18 km, where the maximum effects (20–50 % increase) take place during the winter. In the lower troposphere (up to 8 km), however, the maximum NO_x response occurs during summer time. These seasonal cycles are pronounced in the relative deviation and reflect seasonal behavior of the background abundances of NO_x, which reach minimum values during winter around 100 hPa (~16 km) and during summer in the lower troposphere. On the other hand, the contribution of the energetic particles, that is, GCR, SPE, and EEP in absolute values is seasonally more homogeneous.

Figure 4 illustrates the time evolution of the observed geomagnetic Ap index (red line) and the modeled NO_x produced by the energetic particles (black line) at ~45 km in the southern polar cap (60°–90°S). The shape of the NO_x enhancement closely follows the time series of Ap index showing distinctive spikes in 1994, 2000, 2003, and 2005. However, the magnitude of NO_x enhancement does not agree well with the magnitude of NO_x change obtained from the observation (Randall et al. 2007). In particular, the simulated amount of NO_x produced by the GCR, solar protons, and energetic electrons reach their maximum in 2000, while the observation shows the largest value of NO_x enhancement and Ap index in 2003. It means that the amount of NO_x reaching the stratosphere is modulated by the meteorological conditions and a slower downward propagation in 2003 than in 2000 (not shown) in the experimental run leads to a weaker NO_x enhancement during this year.

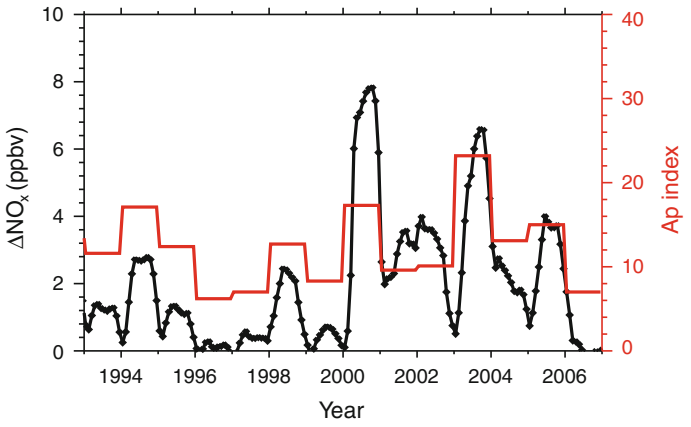

Fig. 4 Time evolution of the annual mean geomagnetic Ap index (*red line*) and the response of zonal mean NO_x (*black line*), (%) to GCR, SPE, and EEP at ~45 km averaged over 60°–90°S

Our results, compared with Baumgaertner et al. (2009), show that the parameterization of the low-energetic electrons is giving good results when comparing with satellite data. Less intensive effects in 2003 can be explained by the application of the "maximum NO_x excess" model by Baumgaertner et al. (2009) for the year 2003.

3.2 Hydrogen Oxides

Figures 5 and 6 illustrate the annual mean zonal mean OH and HO_x ($H + OH + HO_2$) response to the energetic particles as a relative deviation of the experimental run from the reference run. The influx of hydroxyl produced in the thermosphere (>80 km) by EEP was not included in the model due to the short lifetime of this species; therefore, the simulated OH and HO_x change is only due to direct production by SPE and GCR. The simulated OH increase is strongest in the middle stratosphere at about 16 km and in the troposphere going

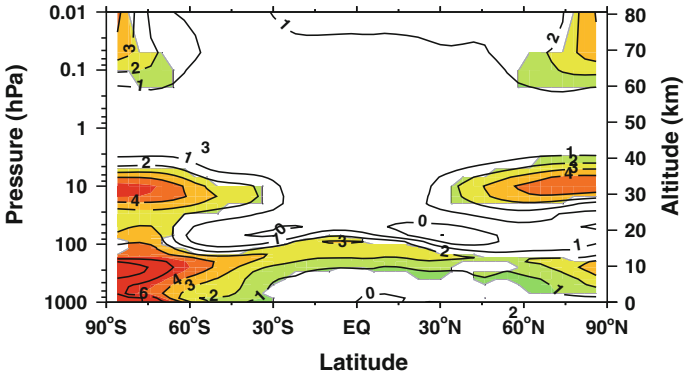

Fig. 5 Annual mean response of zonal mean OH, (%) to GCR, SPE, and EEP. Results are averaged from 1960 to 2005. The *contours* are plotted for: 1, 2, 3, 4, 6, and 8 %. *Color* pattern indicates the regions where the changes are judged statistically significant at or better than 10 % level

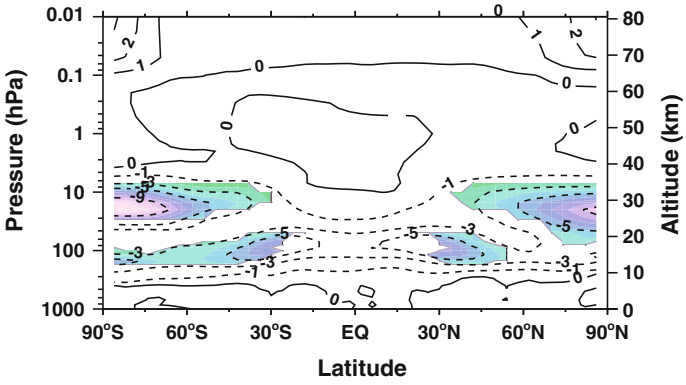

Fig. 6 Annual mean response of zonal mean HO_x, (%) to GCR, SPE, and EEP. Results are averaged from 1960 to 2005. *Solid contours* indicate positive, *dotted contours* negative changes. The *contours* are plotted for: −9, −5, −3, −1, 0, 1, and 2 %. *Color* pattern indicates the regions where the changes are judged statistically significant at or better than 10 % level

from surface up to about 12 km. It was shown by CA11 and SE11 that the production of OH by GCR is not important in the upper stratosphere (~50–60 km) and mesosphere; therefore, the small increase of OH there can be attributed to SPE effects. The OH increase around 10 hPa (~16 km) can be attributed to the combined effects of SPE and GCR. The simulated relative OH increase in the troposphere reaches its maximum in the unpolluted Southern hemisphere and in the uppermost troposphere, where its background concentration is small. The influence of the energetic particles on HO_x is negative in the upper troposphere/lower stratosphere domain because of the reaction chains: $NO_2 + HO_2 \rightarrow HNO_4$ and $NO + HO_2 \rightarrow NO_2 + OH$ followed by $NO_2 + OH + M \rightarrow HNO_3$ (Brasseur and Solomon, 2005). Our model indeed simulates a proper HNO_3 and HNO_4 increase (not shown) confirming these mechanisms. CA11 obtained a similar HO_x depletion due to GCR. A HO_x decrease in the upper troposphere/lower stratosphere was also found by SE11. Due to the absence of precipitating medium-energy-range electrons, which are capable of producing HO_x directly in the mesosphere (>80 km) and the upper stratosphere, our model does not produce the HO_x enhancement in the upper polar atmosphere obtained by SE11. However, the properties of these precipitating electrons are not well known and, at the moment, we do not have solid proof that such events are reasonably frequent and important.

3.3 Ozone and Temperature

The annual mean zonal mean ozone response to the energetic particles as a relative deviation of the experimental run from the reference run is presented in Fig. 7. The combined effect of GCR, SPE, and LEE consist of an ozone depletion going from about 26 km up to 80 km and an ozone increase in the troposphere, that is from the surface up to 12 km. The ozone depletion in the polar mesosphere (60–80 km) and middle stratosphere (~26–32 km) is explained by enhanced NO_x and OH concentrations, which accelerates known catalytical ozone destruction cycles (Brasseur and Solomon 2005; SE11). The ozone depletion in the polar mesosphere is the most pronounced and exceeds 10 % in the uppermost layer. The magnitude of the ozone depletion is substantially lower than the value reported by SE11. It can be explained by much larger OH increase simulated by

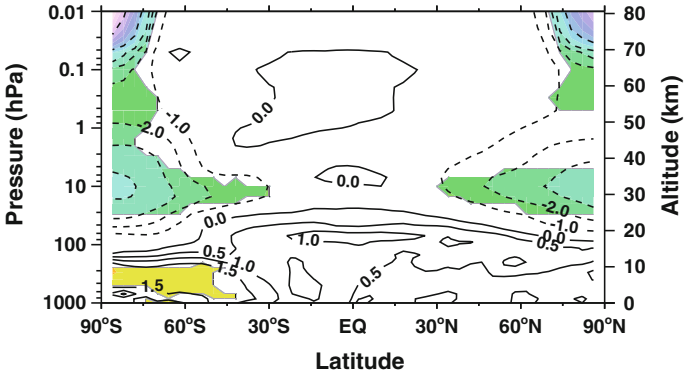

Fig. 7 Annual mean response of zonal mean O_3, (%) to GCR, SPE, and EEP. The *contours* are plotted for: −10.0, −6.0, −4.0, −3.0, −2.0, −1.0, 0.0, 0.5, 1.0, and 1.5 %. Results are averaged from 1960 to 2005. *Solid contours* indicate positive, *dotted contours* negative changes. *Color* pattern indicates the regions where the changes are judged statistically significant at or better than 10 % level

SE11 due to medium-energy-range electron precipitation. The ozone depletion in the middle stratosphere is a combined effect of all precipitating particles. Due to larger NO_x and OH enhancement in the Southern hemisphere, the magnitude of the ozone depletion at an altitude range of approximately 26–32 km is slightly greater, reaching 4 % over the pole. The area of depleted ozone extends to the middle latitudes due to the transport of polar air and local depletion caused by GCR. The simulated ozone depletion in the middle stratosphere is in agreement with SE11 data. The ozone depletion in the lower Northern stratosphere reported by CA11 is not well pronounced in our results probably because of the lower level of chlorine caused by a longer run covering the period from 1960 to 2005.

Additional NO_x in the troposphere (up to 16 km) can lead to an ozone production caused by so-called "photosmog" reactions (Wang et al. 1998; SE11). This "photosmog" reaction starts with the NO_2 photolysis ($NO_2 + hv \rightarrow O + NO$), which is then followed by ozone production through atomic and molecular oxygen recombination. Our model shows a statistical significant change only in the Southern hemisphere, where the natural level of NO_x is very small. The ozone increase there is about 1.5 %, which is smaller and less extended in space than SE11 estimations. As described earlier, the reason for this could be due to underestimated background concentrations of NO_x and O_3 in the model applied by SE11, resulting from both the use of an oversimplified tropospheric chemistry and missing sources of NO_x.

The seasonal march of the O_3 change caused by the energetic particles averaged over the Northern and Southern polar caps (60°–90°) is illustrated in Figs. 8 and 9. In general, the time evolution of the ozone depletion in the mesosphere and the stratosphere follows the time evolution of the NO_x enhancement shown in Figs. 2 and 3, starting with a maximum depletion during the winter and propagating down to the middle stratosphere up to early spring. Therefore, this behavior is related to the NO_x enhancement by the energetic electrons. The secondary maximum in the lower stratosphere in spring and further ozone depletion during spring and summer below 10 hPa ($\sim$32 km) is the result of a combined influence of the energetic electrons, solar protons, and GCR. Similar ozone depletion by up to 4 % during the summer season was also obtained by SE11. In the troposphere, the seasonal cycle differs between the hemispheres. In the Northern hemisphere, statistically

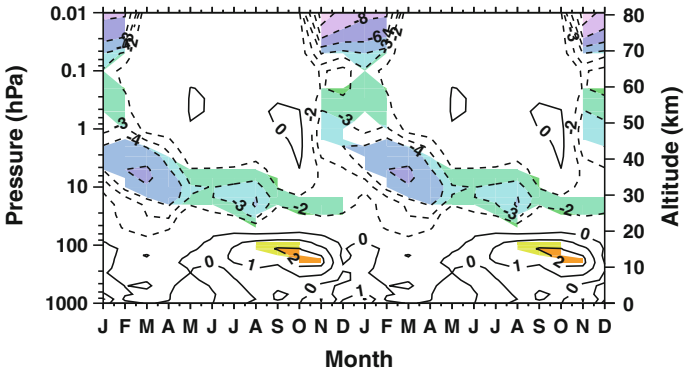

Fig. 8 Monthly mean response of zonal mean O_3, (%) to GCR, SPE, and EEP averaged over 60°–90°N. The *contours* are plotted for: −12.0, −10.0, −8.0, −6.0, −4.0, −3.0, −2.0, 0.0, 1.0, 2.0, and 3.0 %. Results are averaged from 1960 to 2005. *Solid contours* indicate positive, *dotted contours* negative changes. *Color* pattern indicates the regions where the changes are judged statistically significant at or better than 10 % level. Twelve months of the monthly run climatology are repeated

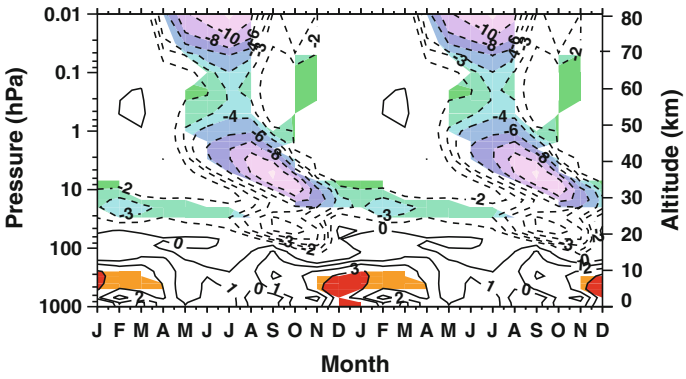

Fig. 9 Same as Fig. 8 but for 60°–90°S

significant ozone enhancement appears during late summer and fall seasons in the upper troposphere, while in the Southern hemisphere, the maximum ozone increase is confined to the middle troposphere and occurs during summer time. This behavior is explained by the seasonal cycle of background NO_x concentrations and availability of sunlight. In the Northern hemisphere, the NO_x-limited regime cannot be reached in the lower stratosphere due to continuous anthropogenic sources of NO_x. In the Southern hemisphere, the background NO_x concentration is always smaller and ozone production maximizes during the summer time when the photolysis of NO_2 is faster.

Ozone is capable of modifying the radiative balance in the atmosphere in short- and longwave spectral ranges. Tropospheric ozone is also an important greenhouse gas. Therefore, the described ozone changes can potentially alter radiative heating, thermal structure, and climate. The simulated monthly mean temperature changes due to the energetic particles over the northern high latitudes are illustrated in Fig. 10. As we can see, the ozone depletion shown in Fig. 8 can lead to some temperature changes varying from 0.5 K cooling in the stratosphere to 0.5 K warming in the mesosphere similar to the

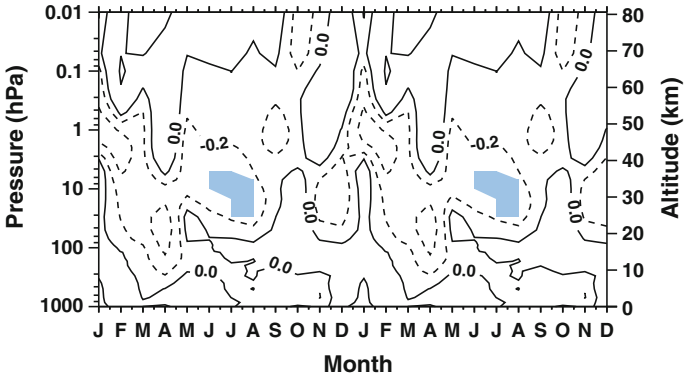

Fig. 10 Monthly mean response of zonal mean temperature, (K) to GCR, SPE, and EEP averaged over 60°–90°N. The *contours* are plotted for: −0.5, −0.2, 0, 0.5, and 0.8 K. Results are averaged from 1960 to 2005. *Solid contours* indicate positive, *dotted contours* negative changes. *Color* pattern indicates the regions where the changes are judged statistically significant at or better than 10 % level. Twelve months of the monthly run climatology are repeated

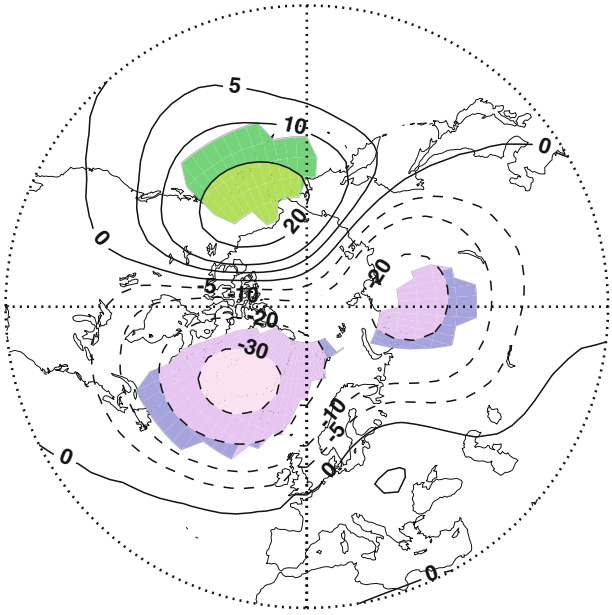

Fig. 11 The response of the geopotential height at 50 hPa, (m) to GCR, SPE, and EEP for boreal winter. Results are averaged from 1960 to 2005. *Solid contours* indicate positive, *dotted contours* negative changes. The *contours* are plotted for: −30, −20, −10, −5, 0, 5, 10, 20 m. *Color* pattern indicates the regions where the changes are judged statistically significant at or better than 10 % level

temperature response obtained by SE11. These changes, however, are not statistically significant in our simulations except for the 0.3 K cooling around 10 hPa (∼32 km) during boreal summer. Nevertheless, such small temperature changes are able to slightly modify the dynamical state of the atmosphere and the strength of the polar vortex. The changes of the geopotential height at 50 hPa shown in Fig. 11 can reach 30 m and reflect an intensification of the polar stratospheric vortex. The downward propagation of this stratospheric perturbation can alter the pattern of the surface air temperature distribution. The details of the involved mechanisms have not been clearly identified (Shepherd, 2002), but the analyses of observational data (e.g., Baldwin and Dunkerton, 2001; Gray et al. 2010) suggest that the stratospheric vortex anomalies are able to propagate down to the troposphere affecting the surface temperature distribution. The response of the surface air temperature during boreal winter season over the Northern hemisphere to GCRs, SPEs, and EEPs is shown in Fig. 12. The pattern of the temperature changes consists of a warming averaged over 46 years of up to 1 K over Europe and a less pronounced warming over Central Russia. Some cooling spots appear over Greenland and the USA. This pattern can be attributed to a more positive phase of the Northern Annular mode. A similar pattern was also found and explained by a high level of geomagnetic activity by Seppälä et al. (2009) using observational data analysis and by Baumgaertner et al. (2011) from model experiments. The smaller magnitude of obtained surface air temperature response can be explained by the fact that we analyzed the response to the multi-year mean geomagnetic activity, while Seppälä et al. (2009) and Baumgaertner et al. (2011) used a composite analysis and analyzed the response during the years with high geomagnetic activity. The warming pattern obtained by Baumgaertner et al. (2011) is confined to northern Europe, while the warming in our simulation covers a wider area including central and southern Europe. The difference can be related to the absence of GCR in the model applied by Baumgaertner et al. (2011). It was pointed out by CA11 that GCR also are able to modify the surface air temperature distribution over Europe.

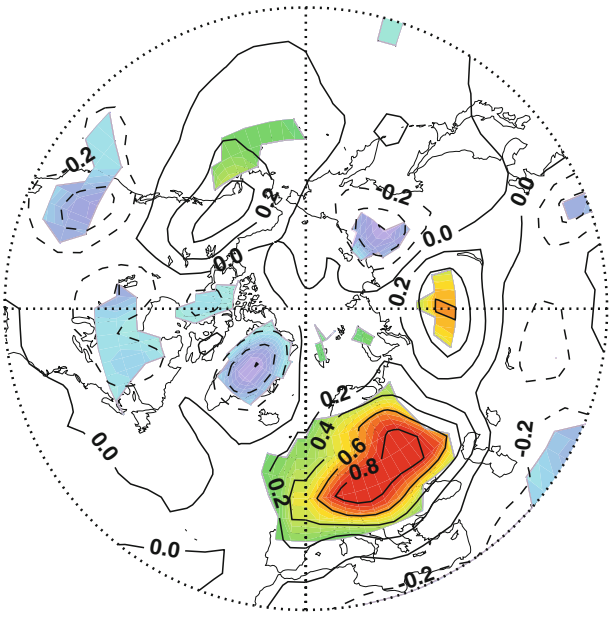

Fig. 12 The response of surface air temperature, (K) to GCR, SPE, and EEP for boreal winter. Results are averaged from 1960 to 2005. *Solid contours* indicate positive, *dotted contours* negative changes. The *contours* are plotted for: −0.6, −0.4, −0.2, 0.0, 0.2, 0.4, 0.6, and 0.8 K. *Color* pattern indicates the regions where the changes are judged statistically significant at or better than 10 % level. The basic reason that the surface temperature response is largest over Europe might be because they are rather sensitive to stratospheric perturbations (see Gray et al. 2010 and references therein)

4 Summary and Outlook

Using the CCM SOCOL v 2.0 in transient mode, we simulate the atmospheric state from 1960 up to 2005 with and without additional sources of NO_x and HO_x caused by three kinds of energetic particles: GCR, SPE, and EEP. We analyze the difference between the climatological states of these runs in order to establish the upper limit of their potential effects on climate. The results show a theoretically expected and consistent response of NO_x, HO_x, ozone, temperature, and dynamics in all considered atmospheric layers. This response consists of substantial increases of NO_x and OH mostly over the polar regions followed by ozone depletion and cooling leading to an intensification of the northern polar vortex and warming over Europe. An ozone increase resulting from GCR has been found in the Southern hemispheric troposphere. Our results are in general agreement with recently published papers (e.g., Calisto et al. 2011; Semeniuk et al. 2011; Baumgaertner et al. 2011) aimed at the understanding of particle precipitation effects on atmospheric chemistry and climate; however, some differences are also evident. Therefore, it is important to incorporate GCR, SPE, and EEP into CCM, which are designed to study atmospheric chemistry, dynamics and climate variability, and trends. Our results emphasize the importance of all types of precipitating particles and of a proper treatment of tropospheric chemistry.

Further efforts should be aimed at the improvement of the representation of energetic particles. For example, Rozanov et al. (2005) demonstrated that high-energy electron precipitation can have a large impact on the atmosphere using a rather simple approach. The comparison of our model results with those of Semeniuk et al. (2011) showed that the medium-energy electron precipitation is important for the simulation of the ozone response. There are some evidences that the frequency of these events is considerable (e.g., Meredith et al. 2011); however, the importance of high-energy electron precipitations still remains questionable (e.g., Sinnhuber et al. 2011). More detailed analysis of observations and modeling efforts are necessary to foster our understanding of these events and to

develop a reliable parameterization of the ionization rates due to high-energy electron precipitation. It is worth noting that CA11 showed a comparable or even larger NH signal for surface temperature in the northern hemisphere due to GCR. Therefore, it is necessary to define which particle class is the most important for the surface climate. However, a proper answer to this question would require a larger set of simulations. The proper identification of the mechanism(s) responsible for the downward propagation of the stratospheric perturbation also remains a fundamental problem. Probably, additional simulations using strong artificial forcing would be necessary to clearly identify the chain of processes.

In the future, more attention should be paid to the prediction of possible changes of energetic particle precipitation. There are some indications that the Sun is entering a phase of low activity. There is a consensus that such a period (similar to Dalton or Maunder minimum) would be characterized by a lower total solar irradiance and higher GCR intensity; however, the changes of frequency and intensity of the electron precipitation events are not clear. Therefore, it is difficult to say whether the expected greenhouse warming will be enhanced or compensated by the decline of solar activity. The important direction of future studies should be the development of a proper model. At the moment, there is no model that is able to simulate all processes relevant to the effects of energetic charged particles on the atmosphere and climate. The existing CCM should be extended up in the vertical direction to treat particle precipitation on a physically solid basis to simulate relevant changes in the ocean dynamics and represent tropospheric chemistry in more detail.

Acknowledgments ER is partially supported by the Swiss National Science Foundation under grant CRSI122-130642 (FUPSOL). TE has received part of her funding from the European Commission's Seventh Framework Programme (FP7/20072013) under the grant agreement no.218816 (SOTERIA, project, http://www.soteria-space.eu). We acknowledge useful discussions within the ISSI Teams on Study of Cosmic Ray Influence upon Atmospheric Processes and Geospace Coupling to Polar Atmosphere.

References

Aikin A (1994) Energetic particle-induced enhancement of stratospheric nitric acid. Geophys Res Lett 21(10):859–862

Baker DN, Barth CA, Mankoff KE, Kanekal SG, Bailey SM, Mason GM, Mazur JE (2001) Relationships between precipitating auroral zone electrons and lower thermospheric nitric oxide densities: 1998–2000. J Geophys Res 106(A11):24465–24480. doi:10.1029/2001JA000078

Baldwin MP, Dunkerton TJ (2001) The solar cycle and stratosphere-troposphere dynamical coupling. Science 294:581–584. doi:10.1126/science.1063315

Barnard L, Lockwood M (2011) A survey of gradual solar energetic particle events. J Geophys Res 116:A05103. doi:10.1029/2010JA016133

Barth CA, Baker DN, Mankoff KD, Bailey SM (2001) The northern auroral region as observed in nitric oxide. Geophys Res Lett 28:1463–1466

Barth CA, Mankoff KD, Balley SM, Solomon SC (2003) Global observations of nitric oxide in the thermosphere. J Geophys Res 108:1027. doi:10.1029/2002JA009458

Baumgaertner AJG, Jöckel P, Brühl C (2009) Energetic particle precipitation in ECHAM5/MESSy1—Part 1: downward transport of upper atmospheric NOx produced by low energy electrons. Atmos Chem Phys 9:2729–2740. doi:10.5194/acp-9-2729-2009

Baumgaertner A, Seppälä A, Jöckel P, Clilverd MA (2011) Geomagnetic activity related NOx enhancements and polar surface air temperature variability in a chemistry climate model: modulation of the NAM index. Atmos Chem Phys 11:4521–4531

Bazilevskaya GA, Usoskin IG, Flückiger EO, Harrison RG, Desorgher L, Bütikofer R, Krainev MB, Makhmutov VS, Stozhkov YI, Svirzhevskaya AK, Svirzhevsky NS, Kovaltsov GA (2008) Cosmic ray induced ion production in the atmosphere. Space Sci Rev 137:149–173

Brasseur GP, Solomon S (2005) Aeronomy of the middle atmosphere. Springer, The Netherlands, p 644
Calisto M, Usoskin I, Rozanov E, Peter T (2011) Influence of galactic cosmic rays on atmospheric composition and dynamics. Atmos Chem Phys 11:4547–4556. doi:10.5194/acp-11-4547-2011
Callis LB, Natarajan M, Evans DS, Lambeth JD (1998) Solar atmospheric coupling by electrons (SOLACE): 1. Effects of the May 12, 1997 solar event on the middle atmosphere. J Geophys Res 103(D21): 28405–28419. doi:10.1029/98JD02408
Cane HV, Mewaldt RA, Cohen CMS, von Rosenvinge TT (2006) Role of flares and shocks in determining solar energetic particle abundances. J Geophys Res 111:A06S90. doi:10.1029/2005JA011071
IPCC (Intergovernmental Panel on Climate Change) (2007) The physical science basis, working group I contribution to the fourth assessment report of the IPCC, Intergovernmental Panel on Climate Change. Cambridge University Press, Cambridge, UK and New York, NY, USA
Clilverd MA, Seppälä A, Rodger CJ, Mlynczak MG, Kozyra JU (2009) Additional stratospheric NOx production by relativistic electron precipitation during the 2004 spring NOx descent event. J Geophys Res 114:A04305. doi:10.1029/2008JA013472
Damiani A, Storini M, Laurenza M, Rafanelli C (2008) Solar particle effects on minor components of the Polar atmosphere. Ann Geophys 26:361–370
Egorova T, Rozanov E, Zubov V, Karol IL (2003) Model for investigating ozone trends (MEZON). Izvestiya Atmos Ocean Phys 39:277–292
Egorova T, Rozanov E, Zubov V, Manzini E, Schmutz W, Peter T (2005) Chemistry-climate model SOCOL: a validation of the present-day climatology. Atmos Chem Phys 5:1557–1576
Egorova T, Rozanov E, Ozolin Y, Shapiro A, Calisto M, Peter T, Schmutz W (2011) The atmospheric effects of October 2003 solar proton event simulated with the chemistry–climate model SOCOL using complete and parameterized ion chemistry. J Atmos Solar Terr Phys 73:356–365. doi:10.1016/j.jastp.2010.01.009
Emery BA, Coumans V, Evans DS, Germany GA, Greer MS, Holeman E, Kadinsky-Cade K, Rich FJ, Xu W (2008) Seasonal, Kp, solar wind, and solar flux variations in long-term single-pass satellite estimates of electron and ion auroral hemispheric power. J Geophys Res 113:A06311. doi:10.1029/2007JA012866
Eyring V, Waugh DW, Bodeker GE, Cordero E, Akiyoshi H, Austin J, Beagley SR, Boville BA, Braesicke P, Brühl C, Butchart N, Chipperfield MP, Dameris M, Deckert R, Deushi M, Frith SM, Garcia RR, Gettelman A, Giorgetta MA, Kinnison DE, Mancini E, Manzini E, Marsh DR, Matthes S, Nagashima T, Newman PA, Nielsen JE, Pawson S, Pitari G, Plummer DA, Rozanov E, Schraner M, Scinocca JF, Semeniuk K, Shepherd TG, Shibata K, Steil B Stolarski RS, Tian W, Yoshiki M (2007) Multimodel projections of stratospheric ozone in the 21st century. J Geophys Res 112:D16303. doi:10.1029/2006JD008332
Funke B, López-Puertas M, Gil-Lopez S, von Clarmann T, Stiller GP, Fischer H, Kellman S (2005) Downward transport of upper atmospheric NOx into the polar stratosphere and lower mesosphere during the Antarctic winter 2003 and Arctic winter 2002/2003. J Geophys Res 112:D24308. doi:10.1029/2005JD006463,2005
Funke B, Baumgaertner A, Calisto M, Egorova T, Jackman CH, Kieser J, Krivolutsky A, López-Puertas M, Marsh DR, Reddmann T, Rozanov E, Salmi S-M, Sinnhuber M, Stiller GP, Verronen PT, Versick S, von Clarmann T, Vyushkova TY, Wieters N, Wissing JM (2011) Composition changes after the "Halloween" solar proton event: the High-Energy Particle Precipitation in the Atmosphere (HEPPA) model versus MIPAS data intercomparison study. Atmos Chem Phys Discuss 11:9407–9514
Gray LJ, Beer J, Geller M, Haigh JD, Lockwood M, Matthes K, Cubasch U, Fleitman D, Harrison G, Hood L, Luterbacher J, Meehl GA, Shindell D, Shindell D, van Geel B, White W (2010) Solar influences on climate. Rev Geophys 48:RG4001. doi:10.1029/2009RG000282
Jackman CH, Marsh DR, Vitt FM, Garcia RR, Fleming EL, Labow GJ, Randall CE, López-Puertas M, Funke B, von Clarmann T, Stiller GP (2008) Short- and medium-term atmospheric constituent effects of very large solar proton events. Atmos Chem Phys 8:765–785. doi:10.5194/acp-8-765-2008
Jackman CH, Marsh DR, Vitt FM, Garcia RR, Randall CE, Fleming EL, Frith SM (2009) Long-term middle atmosphere influence of very large solar proton events. J Geophys Res D114:11304. doi:10.1029/2008JD011415
Lam MM, Horne RB, Meredith NP, Glauert SA, Moffat-Griffin T, Green JC (2010) Origin of energetic electron precipitation $>$ 30 keV into the atmosphere. J Geophys Res 115:A00F08. doi:10.1029/2009JA014619
Langematz U, Grenfell JL, Matthes K, Mieth P, Kunze M, Steil B, Brühl C (2005) Chemical effects in 11-year solar cycle simulations with the Freie Universïtat Berlin Climate Middle Atmosphere Model with online chemistry (FUB-CMAM-CHEM). Geophys Res Lett 32:L13803. doi:10.1029/2005GL022686

López-Puertas M, Funke B, von Clarmann T, Fischer H, Stiller GP (2006) The stratospheric and mesospheric NOy in the 2002–2004 polar winters as measured by MIPAS/ENVISAT. Space Sci Rev 125:403–416. doi:10.1007/s11214-006-9073-2

López-Puertas M, Funke B, Gil-Lopez S, von Clarmann T, Stiller GP, Höpfner M, Kellmann S, Fischer J, Jackman CH (2005) Observation of NOx enhancement and ozone depletion in the Northern and Southern hemispheres after the October–November 2003 solar proton events. J Geophys Res 110: A09S43. doi:10.1029/2005JA011050

Manzini E, McFarlane NA, McLandress C (1997) Impact of the doppler spread parameterization on the simulation of the middle atmosphere circulation using the MA/ECHAM4 general circulation model. J Geophys Res 102:25751–25762

Marsh DR, Garcia RR, Kinnison DE, Boville BA, Sassi F, Solomon SC, Matthes K (2007) Modeling the whole atmosphere response to solar cycle changes in radiative and geomagnetic forcing. J Geophys Res 112:D23306. doi:10.1029/2006JD008306

Meredith NP, Horne RB, Lam MM, Denton MH, Borovsky JE, Green JC (2011) Energetic electron precipitation during high-speed solar wind stream driven storms. J Geophys Res 116:A05223. doi: 10.1029/2010JA016293

Millan RM, Thorne RM (2007) Review of radiation belt relativistic electron losses. J Atmos Solar Terr Phys 69:362–377

Morgenstern O, Giorgetta MA, Shibata K, Eyring V, Waugh DW, Shepherd TG, Akiyoshi H, Austin J, Baumgaertner AJG, Bekki S, Braesicke P, Brühl C, Chipperfield MP, Cugnet D, Dameris M, Dhomse S, Frith SM, Garny H, Gettelman A, Hardiman SC, Hegglin MI, Jöckel P, Kinnison DE, Lamarque JF, Mancini E, Manzini E, Marchand M, Michou M, Nakamura T, Nielsen JE, Olivié D, Pitari G, Plummer DA, Rozanov E, Scinocca JF, Smale D, Teyssedre H, Toohey M, Tian W, Yamashita Y (2010) Review of the formulation of present-generation stratospheric chemistry-climate models and associated external forcings. J Geophys Res 115:D00M02. doi:10.1029/2009jd013728

Porter HS, Jackman CH, Green AES (1976) Efficiencies for production of atomic nitrogen and oxygen by relativistic proton impact in air. J Chem Phys 65:1

Randall CE, Harvey VL, Singleton CS, Bailey SM, Bernath PF, Codrescu M, Nakajima H, Russell JM (2007) Energetic particle precipitation effects on the Southern Hemisphere stratosphere in 1991–2005. J Geophys Res 112:D08308. doi:10.1029/2006JD007696

Reames D (1999) Particle acceleration at the sun and in the heliosphere. Space Sci Rev 90:413–491

Reddmann T, Ruhnke R, Versick S, Kouker W (2010) Modeling disturbed stratospheric chemistry during solar-induced NOx enhancements observed with MIPAS/ENVISAT. J Geophys Res 115:D00I11. doi: 10.1029/2009JD012569

Richardson IG, Cliver EW, Cane HV (2000) Sources of geomagnetic activity over the solar cycle: relative importance of coronal mass ejections, high-speed streams, and slow solar wind. J Geophys Res 105(A8):18203–18213

Rozanov E, Schlesinger ME, Zubov V, Yang F, Andronova NG (1999) The UIUC three-dimensional stratospheric chemical transport model: Description and evaluation of the simulated source gases and ozone. J Geophys Res 104:11755–11781

Rozanov E, Callis L, Schlesinger M, Yang F, Andronova N, Zubov V (2005) Atmospheric response to NOy source due to energetic electron precipitation. Geophys Res Lett 32:L14811. doi:10.1029/2005GL023041

Rusch D, Gerard G-C, Solomon S, Crutzen P, Reid G (1981) The effect of particle precipitation events on the neutral and ion chemistry of the middle atmosphere. 1. Odd nitrogen. Planet Space Sc 29:767–774

Schraner M, Rozanov E, Schnadt Poberaj C, Kenzelmann P, Fischer AM, Zubov V, Luo BP, Hoyle CR, Egorova T, Fueglistaler S, Brönnimann S, Schmutz W, Peter T (2008) Technical note: chemistry-climate model SOCOL: version2.0 with improved transport and chemistry/micro-physics schemes. Atmos Chem Phys 8:5957–5974

Semeniuk K, Fomichev VI, McConnell JC, Fu C, Melo SML, Usoskin IG (2011) Middle atmosphere response to the solar cycle in irradiance and ionizing particle precipitation. Atmos Chem Phys 11:5045–5077

Seppälä A, Verronen PT, Clilverd MA, Randall CE, Tamminen J, Sofieva V, Backman L, Kyrölä E (2007a) Arctic and Antarctic polar winter NOx and energetic particle precipitation in 2002–2006. Geophys Res Lett 34:L12810. doi:10.1029/2007GL029733

Seppälä A, Clilverd MA, Rodger CJ (2007b) NOx enhancements in the middle atmosphere during 2003–2004 polar winter: Relative significance of solar proton events and the aurora as a source. J Geophys Res 112:D23303. doi:10.1029/2006JD008326

Seppälä A, Randall CE, Clilverd MA, Rozanov E, Rodger CJ (2009) Geomagnetic activity and polar surface air temperature variability. J Geophys Res 114:A10312. doi:10.1029/2008JA014029

Shepherd TG (2002) Issues in stratosphere-troposphere coupling. J Meteorol Soc Jpn 80:769–792. doi:10.2151/jmsj.80.769

Sinnhuber M, Kazeminejad S, Wissing JM (2011) Interannual variation of NOx from the lower thermosphere to the upper stratosphere in the years 1991–2005. J Geophys Res 116:A02312. doi:10.1029/2010JA015825

Siskind DE, Nedoluha GE, Randall CE, Fromm M, Russell JM III (2000) An assessment of Southern Hemisphere stratospheric NOx enhancements due to transport from the upper atmosphere. Geophys Res Lett 27(3):329–332. doi:10.1029/1999GL010940

Solomon S, Rusch DW, Gerard J-C, Reid GC, Crutzen PJ (1981) The effect of particle precipitation events on the neutral and ion chemistry of the middle atmosphere, II, Odd hydrogen. Planet Space Sci 29(8): 885–892

SPARC CCMVal (2010) SPARC report on the evaluation of chemistry-climate models In: Eyring V, Shepherd TG, Waugh DW (eds) SPARC, Toronto, Ontario, Canada, Tech. Rep. WCRP-132/WMO/TD-1526/SPARC Rep, p 5

Turunen E, Verronen PT, Seppälä A, Rodger CJ, Clilverd MA, Tamminen J, Enell CF, Ulich T (2009) Impact of different energies of precipitating particles on NOx generation in the middle and upper atmosphere during geomagnetic storms. J Atmos Sol Terr Phy 71:1176–1189. doi:10,1016/j.jastp.2008.07.05

Usoskin IG, Kovaltsov GA (2006) Cosmic ray induced ionization in the atmosphere: Full modeling and practical applications. J Geophys Res 111:D21206. doi:10.1029/2006JD007150

Usoskin IG, Kovaltsov GA, Mironova IA (2010) Cosmic ray induced ionization model CRAC:CRII: An extension to the upper atmosphere. J Geophys Res 115:D10302. doi:10.1029/2009JD013142

Verronen PT, Rodger CJ, Clilverd MA, Wang S (2011) First evidence of mesospheric hydroxyl response to electron precipitation from the radiation belts. J Geophys Res 116:D07307. doi:10.1029/2010JD014965

Wang Y, Jacob DJ, Logan JA (1998) Global simulation of tropospheric O_3-NO_x-hydrocarbon chemistry, 3. Origin of tropospheric ozone and effects of non-methane hydrocarbons. J Geophys Res 103: 10757–10767

Wissing JM, Kallenrode M-B, Wieters N, Winkler H, Sinnhuber M (2010) Atmospheric ionization module Osnabrück (AIMOS): 2. Total particle inventory in the October–November 2003 event and ozone. J Geophys Res 115:A02308. doi:10.1029/2009JA014419